

Nonlinear Numerical Simulation of Reinforced Concrete Columns Under Cyclic Biaxial Bending Moment and Axial Loading

Kabir Sadeghi¹

Received: 10 August 2014/Revised: 23 September 2015/Accepted: 11 October 2015/Published online: 2 June 2016
© Iran University of Science and Technology 2016

Abstract A nonlinear finite element algorithm is proposed to analyze the reinforced concrete (RC) columns subjected to cyclic biaxial bending moment and axial loading. In the proposed algorithm, the following parameters are considered: uniaxial behavior of concrete and steel elements, the pseudo-plastic hinge produced in the critical sections, and global behavior of the columns. In the proposed numerical simulation, the column is discretized into two macro-elements located between the pseudo-plastic hinges at critical sections and the inflection point. The critical sections are discretized into fixed rectangular finite elements. The basic equilibrium is justified over a critical hypothetical cross section assuming the kinematics Navier's hypothesis with an average curvature. The method used qualifies as a "strain plane control process" that requires the resolution of a quasi-static simultaneous equation system using a triple iteration process over the strains in each section. To reach equilibrium, three main strain parameters (the strains in the extreme compressive point, the strains in the extreme tensile point and the strains in another corner of the section) are used as the three main variables. The proposed algorithm has been validated by the results of tests carried out on full-scale RC columns. The application of the components effects combination method is also compared with the proposed simultaneous direct method. The results obtained show the necessity of applying SDM for the post-elastic phase, which occurs frequently during earthquake loading.

Keywords Numerical simulation · Reinforced concrete · Column · Cyclic loading · Biaxial bending moment

1 Introduction

A range of approaches has been used to analyze the behavior of RC sections under biaxial bending moment and axial loading (BBMAL). The simplified models of the earlier approaches do not reflect the nonlinearity of materials. Richard Yen [1] has proposed a model to calculate RC sections under biaxial bending moment (BBM) based on the position of the neutral axis and the percentage of longitudinal reinforcement. In this method, many simplifications are used that have a detrimental effect on the precision of the results. Yau et al. [2] have proposed a method to calculate the ultimate strength of the sections under BBM using the percentage of longitudinal reinforcement and the distance between the neutral axis and the point with maximum compressive stress as main parameters. Alnoury et al. [3] have proposed a method using the tangent of the force–displacement curve and the local stiffness in the section level. The model proposed by Hsu et al. [4], which uses the developed Newton–Raphson method and simplified models of strain–stress curves for concrete and reinforcement, is not applicable for the descending branch of the moment–curvature ($M-\phi$) curve. Brondum-Nielsen [5] has proposed a method to calculate the ultimate strength of the sections under BBM using the developed Newton–Raphson method and simplified rectangular model of strain–stress for concrete recommended by the CEB-FIP code. Zak [6] has also proposed a method to calculate the ultimate strength of the sections under BBM using the developed Newton–Raphson method. The Newton–Raphson method yields a fast solution, but

✉ Kabir Sadeghi
kabir.sadeghi@neu.edu.tr; kabirsadeghi@gmail.com

¹ Civil Engineering Department, Near East University, TRNC, Mersin 10, Nicosia, Turkey

presents problems while passing the peak point of the response curve and near the inflection point that causes divergence of the solution. Newton’s method is well adapted for monotonic curves and needs to be transformed at each relative extreme point occurrence. The maxima have to be evaluated anyway. The Ricks method is derived from Newton’s and allows the user to cross over the peaks. Newton and Ricks processes must be used with caution in numerical simulation. Some methods such as those proposed by Amziane [7] are applicable to RC structures under uniaxial cyclic bending with axial load.

Among several existing techniques, used to analyze RC sections under BBMAL, two are the most common. Direct search procedures are used to determine either the strain equilibrium plane or the location of the neutral axis.

Except for the case of the linear approach where exact integration rules can be used, the section can be discretized into parallel layers rotating parallel to the neutral axis. This method can be applied only in the monotonic loading case. Another approach is to discretize the cross section into FRFE. This method can be used under any cyclic or monotonic loading cases.

The aim of this paper is to present a numerical simulation algorithm to assess the behavior of RC columns under CBBMAL. This is achieved using ME and FRFE in the discretization of the column and the sections based on the local degradation of materials.

2 Proposed Numerical Simulation Approach

2.1 Description of the Proposed Algorithm

In the proposed simulation algorithm, the column is decomposed into two ME positioned between the inflection point (zero moment) and critical sections (maximum moments). Then the nonlinear behavior of ME is analyzed. In fact, a macro-element acts as a fixed bottom-free top half-column under biaxial cyclic bending moment (i.e., cyclic lateral force in any direction) with axial load. Finally, the two connected ME are assembled to determine the global behavior of the column.

To find the status of the entire column, the applied loads and also the secondary moments, due to P-Δ effect, are considered in the simulation of the column.

In the proposed algorithm, for each concrete and reinforcement element, a uniaxial behavior is considered and their strain distributions are assumed to form a plane which remains a plane during deformation (kinematics Navier’s hypothesis). The stresses of concrete and steel are expressed as nonlinear functions of strains (ϵ) in each (i, j) concrete and (k) steel elements (see Fig. 1). For compressive

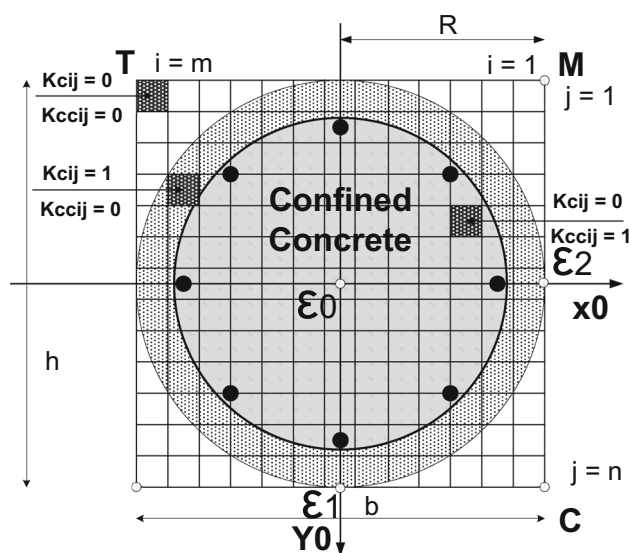


Fig. 1 Discretization of a column’s section

confined and unconfined concrete elements, the author’s cyclic stress–strain model [8–10] and for reinforcements the expression proposed by Park and Kent [11] based on the Ramberg–Osgood cyclic model have been used in the proposed simulation algorithm. The concrete tensile stress is assumed to be linear up to the concrete tensile strength. To determine the maximum compression strain value (ϵ_{CU}) of unconfined concrete, Eq. (1) given by the CEB Code [12] was used. This equation is particularly applicable when there is a loss of concrete cover outside the stirrups:

$$\epsilon_{CU} = (4 - 0.02f'_c)/1000 \quad (f'_c \text{ in MPa}), \tag{1}$$

where f'_c represents 28 days’ compressive strength of unconfined concrete.

To determine the failure of confined concrete situated inside the stirrups, in the proposed simulation, Eq. (2) proposed by Sheikh [13] was used:

$$\epsilon_{CCU} = 0.004 + (0.9\rho_s \cdot f_{yh})/300 \quad (f_{yh} \text{ in MPa}), \tag{2}$$

where ϵ_{CCU} presents the maximum compression strain value of confined concrete, ρ_s the ratio of transversal reinforcement volume per concrete volume situated inside the stirrups and f_{yh} the yielding stress of the stirrups.

The basic equilibrium is justified over a critical hypothetical cross section, assuming the Navier law with an average curvature. The method used qualifies as a “strain plane control process” that requires the resolution of a quasi-static simultaneous equation system using a triple iteration process over the strains. The calculations are based on the cyclic nonlinear stress–strain relationships for concrete and reinforcement FE. To reach equilibrium, three main strain parameters ϵ_C (the strains in the extreme

compressive point), ε_T (the strains in the extreme tensile point) and ε_M (the strains in the point M located at another corner of the section) are used as three main variables as shown in Fig. 1. For non-rectangular sections, these points C, T and M may be outside the actual cross sections and be located on the discretizing mesh frontiers.

2.2 Discretization Principles

The critical sections are discretized into FRFE. Since to follow up on the loading-unloading paths in the simulation, the last three loading-unloading steps should be recorded, the FRFE discretization with the fixed center of gravity positions for elements has been employed.

2.3 Equilibrium Conditions

2.3.1 Quasi-static Equilibrium of the Section

The fundamental relationships determining the equilibrium state of the sections are as follows:

- a) equilibrium equation of axial forces in the center of the column’s section,
- b) equilibrium equations of bending moments at the column’s section.

The general equilibrium system of each section consists of three nonlinear relations equating the external and internal effects:

$$N_{\text{ext}} = N_{\text{int}}, \tag{3}$$

$$Mx_{\text{ext}} = Mx_{\text{int}}, \tag{4}$$

$$My_{\text{ext}} = My_{\text{int}}, \tag{5}$$

where:

$$M_{\text{ext}} = [(Mx_{\text{ext}})^2 + (My_{\text{ext}})^2]^{1/2}, \tag{6}$$

$$M_{\text{int}} = [(Mx_{\text{int}})^2 + (My_{\text{int}})^2]^{1/2}, \tag{7}$$

in which N_{ext} and N_{int} represent the external and internal axial forces, respectively; Mx_{ext} , My_{ext} , Mx_{int} and My_{int} represent the external and internal bending moments about the orthogonal x_0 and y_0 axes passing through the centroid of the cross section, respectively (see Fig. 1); M_{ext} and M_{int} represent the total external and internal bending moments. Mx_{int} and My_{int} are defined in Sect. 2.3.2 below.

The proposed method requires the resolution of a quasi-static simultaneous equations system using a triple iteration process over the strains which depends on the position of the neutral axis. It is based also on the non-linear stress–strain relationships for concrete and reinforcement FE.

2.3.2 Quasi-static Equilibrium of the Section

The internal efforts are as follows:

$$N_{\text{int}} = \sum_i^m \sum_j^n Kc_{ij} \cdot \sigma_{cc_{ij}} \cdot A_{ij} + \sum_i^m \sum_j^n Kc_{ij} \cdot \sigma_{c_{ij}} \cdot A_{ij} + \sum_k^{ns} \sigma_{s_k} \cdot As_k, \tag{8}$$

$$Mx_{\text{int}} = \sum_i^m \sum_j^n Kc_{ij} \cdot \sigma_{cc_{ij}} \cdot y_{ij} \cdot A_{ij} + \sum_i^m \sum_j^n Kc_{ij} \cdot \sigma_{c_{ij}} \cdot y_{ij} \cdot A_{ij} + \sum_k^{ns} \sigma_{s_k} \cdot y_k \cdot As_k, \tag{9}$$

$$My_{\text{int}} = \sum_i^m \sum_j^n Kc_{ij} \cdot \sigma_{cc_{ij}} \cdot x_{ij} \cdot A_{ij} + \sum_i^m \sum_j^n Kc_{ij} \cdot \sigma_{c_{ij}} \cdot x_{ij} \cdot A_{ij} + \sum_k^{ns} \sigma_{s_k} \cdot x_k \cdot As_k, \tag{10}$$

where $\sigma_{cc_{ij}}$, $\sigma_{c_{ij}}$ and σ_{s_k} represent the stresses of confined concrete, unconfined concrete and steel FE, respectively; A_{ij} and As_k represent the concrete and steel element areas. The Kc_{ij} and Kc_{ij} factors are used to indicate whether the (i, j) element belongs to the confined concrete, unconfined concrete or a virtual part of the section and also show the status of concrete cover. $Kc_{ij} = 1$, for a confined concrete element and $Kc_{ij} = 1$, for an unconfined concrete element. $Kc_{ij} = 0$ and $Kc_{ij} = 0$ for the other virtual elements in the case of non-rectangular section, or for the elements when fail; ns is the total number of longitudinal reinforcement in the section; $m = i_{\text{max}}$ and $n = j_{\text{max}}$. For a nonrectangular section, a virtual rectangular grid section is assumed [9] (see Fig. 1).

To reach equilibrium, three main characteristic parameters ε_C , ε_T and ε_M are used as the three main unknown variables.

2.4 Determination of Strains

The strains in the concrete and steel FE are calculated by applying the following equations:

$$\varepsilon_{ij} = \varepsilon_0 + \phi_x(x_{ij} - x_0) + \phi_y(y_{ij} - y_0), \tag{11}$$

$$\varepsilon_{s_k} = \varepsilon_0 + \phi_x(xs_k - x_0) + \phi_y(ys_k - y_0), \tag{12}$$

with:

$$\varepsilon_0 = \frac{\varepsilon_C + \varepsilon_T}{2}, \tag{13}$$

where ε_0 represents the strain of the section’s centroid with coordinates of (x_0, y_0) ; ϕ_x and ϕ_y represent the curvatures in the two main axes of the section (see Sect. 2.5 below).

2.5 Determination of Curvatures

The curvatures in directions x and y are calculated as follows:

$$\phi_x = \frac{(\varepsilon_2 - \varepsilon_0)}{(b/2)}, \quad (14)$$

$$\phi_y = \frac{(\varepsilon_1 - \varepsilon_0)}{(h/2)}, \quad (15)$$

with:

$$\varepsilon_2 = \frac{\varepsilon_C + \varepsilon_M}{2}, \quad (16)$$

$$\varepsilon_1 = \varepsilon_C + \frac{\varepsilon_T}{2} - \frac{\varepsilon_M}{2}, \quad (17)$$

where b and h represent the smaller and larger dimensions of the section, respectively.

The maximum curvature is given as:

$$\phi = \frac{\varepsilon_C}{h'}, \quad (18)$$

where h' represents the distance between the extreme compression point C and the neutral axis.

It can be proved that this maximum curvature can be also presented as:

$$\phi = \sqrt{\phi_x^2 + \phi_y^2}. \quad (19)$$

2.6 Determination of the Neutral Axis Position

The coordinates of the neutral axis intersections with x_0 and y_0 axes are found from Eqs. (20) and (21):

$$x_n = \frac{b}{2} + \left(\frac{h}{2}\right) \left(\frac{\phi_y}{\phi_x}\right) - \frac{\varepsilon_C}{\phi_x}, \quad (20)$$

$$y_n = \frac{h}{2} + \left(\frac{b}{2}\right) \left(\frac{\phi_x}{\phi_y}\right) - \frac{\varepsilon_C}{\phi_y}. \quad (21)$$

2.7 Loading and Stress–Strain Histories

The loading history of concrete and steel FE on the stress–strain curves are saved and compared. This is not only related to the loading history, but also to the position of the FE on the sections. Each step of loading of ME, concrete FE and steel FE are saved to compare with the two previous steps.

2.7.1 Loading History on Sections and ME

Based on the applied external moment or applied relative curvature on the section l for loading step k

“ $M_{\text{ext}}(k, l)$ or $\phi(k, l)$ ”, the parameters “ $dM1$ and $dM2$ ” or “ $d\phi1$ and $d\phi2$ ” are defined as follows.

For the imposed force case:

$$dM1 = M_{\text{ext}}(k-1, l) - M_{\text{ext}}(k-2, l), \quad (22)$$

$$dM2 = M_{\text{ext}}(k, l) - M_{\text{ext}}(k-1, l). \quad (23)$$

For the imposed curvature (or imposed displacement) case:

$$d\phi1 = \phi(k-1, l) - \phi(k-2, l), \quad (24)$$

$$d\phi2 = \phi(k-1, l) - \phi(k-2, l). \quad (25)$$

These parameters allow following up the different phases of loading history on the sections. The four different typical trajectories are as follows:

Phase 1—loading:

For the imposed force case:

$$[dM1 \geq 0 \text{ and } dM2 > 0]. \quad (26)$$

For the imposed curvature (or imposed displacement) case:

$$[d\phi1 \geq 0 \text{ and } d\phi2 > 0]. \quad (27)$$

Phase 2—unloading after loading:

For the imposed force case:

$$[dM1 \geq 0 \text{ and } dM2 < 0]. \quad (28)$$

For the imposed curvature (or imposed displacement) case:

$$[d\phi1 \geq 0 \text{ and } d\phi2 < 0]. \quad (29)$$

Phase 3—Unloading:

For the imposed force case:

$$[dM1 < 0 \text{ and } dM2 < 0]. \quad (30)$$

For the imposed curvature (or imposed displacement) case:

$$[d\phi1 < 0 \text{ and } d\phi2 < 0]. \quad (31)$$

Phase 4—reloading after unloading:

For the imposed force case:

$$[dM1 < 0 \text{ and } dM2 > 0]. \quad (32)$$

For the imposed curvature (or imposed displacement) case:

$$[d\phi1 < 0 \text{ and } d\phi2 > 0]. \quad (33)$$

2.7.2 Loading History of Concrete and Steel FE

Each concrete or steel FE has its own proper loading history. For example, on a section, some FE may be under loading, and at the same time some other FE may be under the unloading or reloading phase.

Based on the strain of finite element ij of section l for the step k of the loading “ $\varepsilon(k, l, i, j)$ ”, the parameters of $d\varepsilon_1$ and $d\varepsilon_2$ are defined as follows:

$$d\varepsilon_1 = \varepsilon(k - 1, l, i, j) - \varepsilon(k - 2, l, i, j), \tag{34}$$

$$d\varepsilon_2 = \varepsilon(k, l, i, j) - \varepsilon(k - 1, l, i, j). \tag{35}$$

These parameters allow fixing the limits given for the iteration process to research the equilibrium parameters. The four different typical phases are as follows:

Loading phase:

$$d\varepsilon_1 \geq 0 \text{ and } d\varepsilon_2 > 0]. \tag{36}$$

Unloading after loading phase:

$$d\varepsilon_1 \geq 0 \text{ and } d\varepsilon_2 < 0]. \tag{37}$$

Unloading phase:

$$d\varepsilon_1 < 0 \text{ and } d\varepsilon_2 < 0]. \tag{38}$$

Reloading after unloading phase:

$$d\varepsilon_1 < 0 \text{ and } d\varepsilon_2 > 0]. \tag{39}$$

An example of loading–unloading path for confined concrete FE is shown in Fig. 2.

The same procedure is used for the loading history of steel FE.

An example of loading–unloading path for steel FE is shown in Fig. 3.

2.8 Determination of the Equilibrium Parameters Limits

In each step of loading for a fixed value of ε_C , the value of ε_T is situated between ε_{Tmin} and ε_{Tmax} , while ε_M is always between ε_C and ε_T .

$$\varepsilon_{Tmin} \leq \varepsilon_T \leq \varepsilon_{Tmax}, \tag{40}$$

$$\varepsilon_{Cmin} \leq \varepsilon_C \leq \varepsilon_{Cmax}. \tag{41}$$

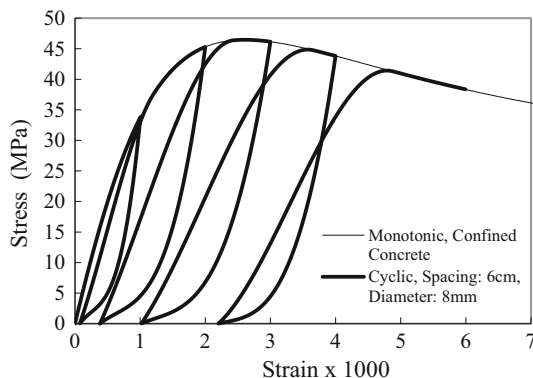


Fig. 2 An example of the loading–unloading path for confined concrete FE

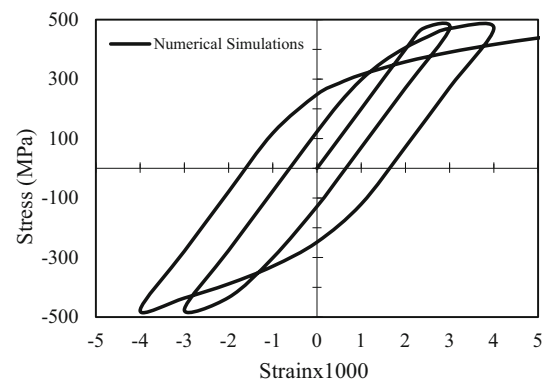


Fig. 3 An example of the loading–unloading path for steel FE

In loading or reloading cases:

$$\varepsilon_T \leq \varepsilon_M \leq \varepsilon_C. \tag{42}$$

In unloading cases:

$$\varepsilon_T \geq \varepsilon_M \geq \varepsilon_C. \tag{43}$$

The determination of these terminal iterations is performed based on the loading history in the following manner:

For the initial loading:

$$\varepsilon_{Cmax} = +0.003, \tag{44}$$

$$\varepsilon_{Cmin} = -0.020, \tag{45}$$

$$\varepsilon_{Tmax} = +0.003, \tag{46}$$

$$\varepsilon_{Tmin} = -0.020. \tag{47}$$

For the loading or reloading cases:

$$\varepsilon_{Cmax} = +0.003, \tag{48}$$

$$\varepsilon_{Cmin} = -0.050 \text{ or } \varepsilon_C(k - 1), \tag{49}$$

$$\varepsilon_{Tmax} = +0.030 \text{ or } \varepsilon_T(k - 1), \tag{50}$$

$$\varepsilon_{Tmin} = -0.050. \tag{51}$$

For the unloading cases:

$$\varepsilon_{Cmax} = +0.003 \text{ or } \varepsilon_C(k - 1), \tag{52}$$

$$\varepsilon_{Cmin} = -0.050, \tag{53}$$

$$\varepsilon_{Tmax} = +0.030, \tag{54}$$

$$\varepsilon_{Tmin} = -0.050 \text{ or } \varepsilon_T(k - 1). \tag{55}$$

2.9 Determination of the Equilibrium Parameters (ε_C , ε_T and ε_M)

For the strain in the extreme compression point of the section:

$$\varepsilon_C = (\varepsilon_{Cmin} + \varepsilon_{Cmax})/2. \tag{56}$$

For the strain in the extreme tension point of the section:

$$\varepsilon_T = (\varepsilon_{Tmin} + \varepsilon_{Tmax})/2. \tag{57}$$

For the strain in point M:

$$\varepsilon_M = (\varepsilon_{Mmin} + \varepsilon_{Mmax})/2. \tag{58}$$

The initial values for ε_{Mmin} and ε_{Mmax} can be considered as ε_T and ε_C , respectively.

2.10 Verification of the Equilibrium Between the External and Internal Efforts

To follow up on the verification procedure of the equilibrium between the external and internal orientation angles Ω [Ω equals the angle between the resultant moment M and the moment component M_x , see Eq. (63)], axial forces and moments (see the main part of the simulation flowchart in Fig. 4), an iteration process over the strains is carried out as follows.

2.10.1 Verification of the Equilibrium Between the External and Internal Orientation Angles

The equilibrium between the imposed external and internal orientation angles Ω is verified by performing an iteration process over the strains of point M on the section (ε_M) for the given values of ε_C and ε_T as follows:

$$\varepsilon_{Mmin} = \varepsilon_M \quad (\text{for } \Omega_{ext} > \Omega_{int}), \tag{59}$$

$$\varepsilon_{Mmax} = \varepsilon_M \quad (\text{for } \Omega_{ext} < \Omega_{int}). \tag{60}$$

In the next iteration ($i + 1$)th, the following equation is applied:

$$\varepsilon_{M(i+1)} = (\varepsilon_{Mmin(i)} + \varepsilon_{Mmax(i)})/2. \tag{61}$$

By calculating the strains and stresses of concrete and steel FE, internal moments and orientation angles, and verification of the equilibrium of external and internal efforts during a set of the successive iteration process, this should conform to the following equilibrium condition:

$$\Omega_{ext} = \Omega_{int}, \tag{62}$$

where:

$$\Omega_{ext} = \text{Tan}^{-1}(My_{ext}/Mx_{ext}), \tag{63}$$

$$\Omega_{int} = \text{Tan}^{-1}(My_{int}/Mx_{int}). \tag{64}$$

2.10.2 Verification of the Equilibrium Between the External and Internal Axial Forces

The equilibrium between the imposed external and internal axial forces is verified by performing an iteration process over the strains of extreme tension point T on the section (ε_T) for the given value of ε_C as follows:

$$\varepsilon_{Tmin} = \varepsilon_T \quad (\text{for } N_{ext} > N_{int}), \tag{65}$$

$$\varepsilon_{Tmax} = \varepsilon_T \quad (\text{for } N_{ext} < N_{int}). \tag{66}$$

In the next iteration ($i + 1$)th, the following equation is applied:

$$\varepsilon_{T(i+1)} = (\varepsilon_{Tmin(i)} + \varepsilon_{Tmax(i)})/2. \tag{67}$$

By calculating the strains and stresses of concrete and steel FE, the internal moments, the internal orientation angles and the internal axial forces are calculated. Then, the equilibrium of external and internal efforts, employing a set of the successive iteration process, is verified. This should conform to the following equilibrium condition:

$$N_{ext} = N_{int}. \tag{68}$$

2.10.3 Verification of the Equilibrium Between the External and Internal Moments

The equilibrium between the imposed external and internal moments is verified by performing an iteration process over the strains of extreme compression point C as follows:

$$\varepsilon_{Cmin} = \varepsilon_C \quad (\text{for } M_{int} > M_{ext}), \tag{69}$$

$$\varepsilon_{Cmax} = \varepsilon_C \quad (\text{for } M_{int} < M_{ext}). \tag{70}$$

In the next iteration ($i + 1$)th, the following equation is applied:

$$\varepsilon_{C(i+1)} = (\varepsilon_{Cmin(i)} + \varepsilon_{Cmax(i)})/2. \tag{71}$$

By calculating the strains and stresses of concrete and steel FE, the internal moments, the internal orientation angles and the internal axial forces are calculated. Then the equilibrium of external and internal efforts, employing a set of the successive iteration process, is verified. This should conform to the following equilibrium condition:

$$M_{ext} = M_{int}. \tag{72}$$

3 Convergence Criteria

To achieve an acceptable accuracy within a reasonable calculation time, the convergence tolerances are considered as:

$$|\Omega_{ext} - \Omega_{int}| \leq 0.1^\circ, \tag{73}$$

$$|N_{ext} - N_{int}| \leq 0.001|N_{ext}|, \tag{74}$$

$$|M_{ext} - M_{int}| \leq 0.001|M_{ext}|. \tag{75}$$

3.1 Calculation of Deflections

In the proposed simulation, two methods are used to calculate the deflections: curvatures numerical double

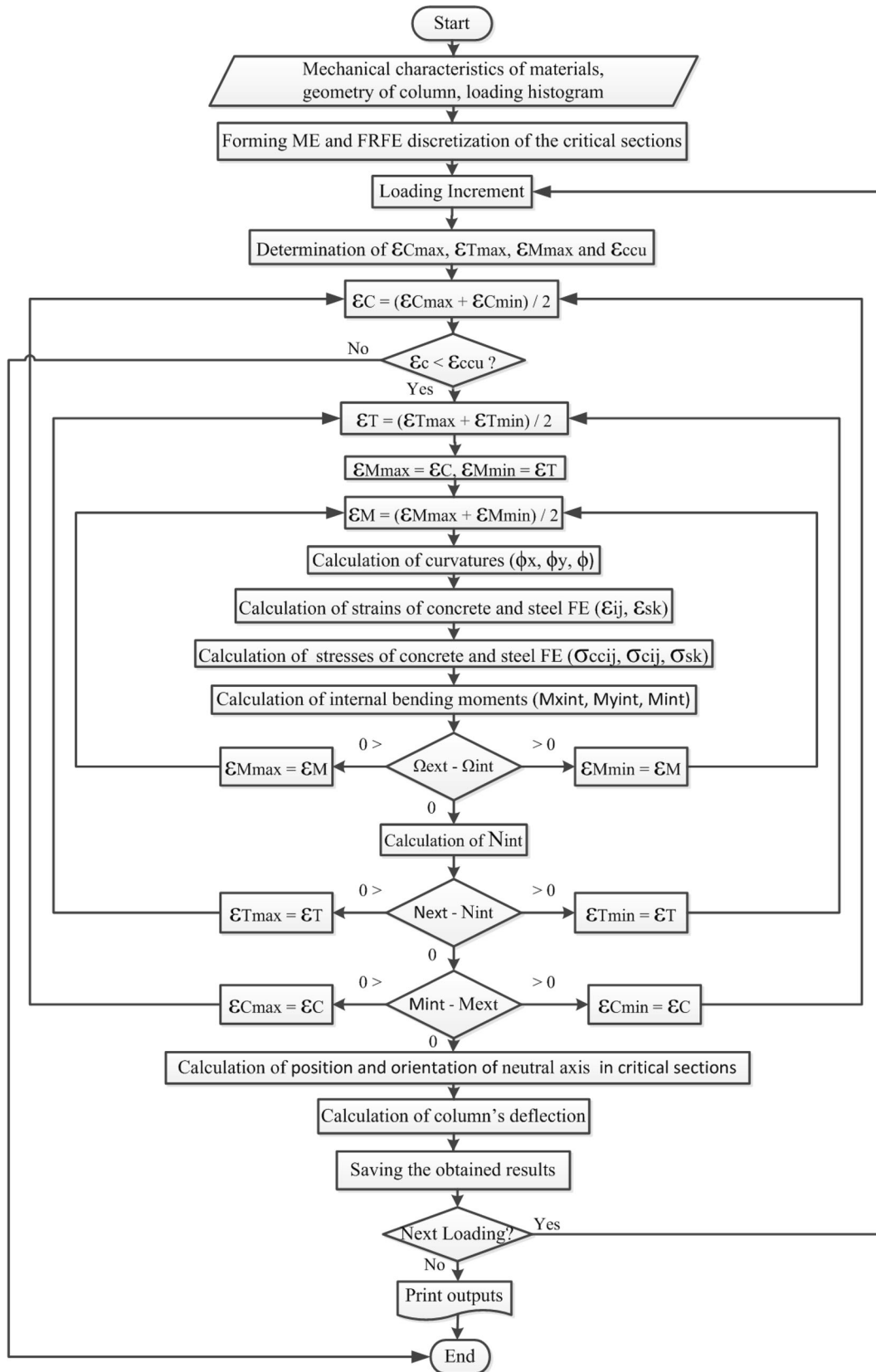


Fig. 4 Flowchart of the main parts of the simulation of columns under CBBMAL

integration method (CNDIM) and elasto-plastic method (EPM). In CNDIM, the equilibrium state is found in each cross section discretized along the length of the column and then a numerical double integration of curvatures ϕ_x and ϕ_y is performed. To apply CNDIM, Eqs. (76) and (77), proposed by Lamirault and Bresse [14], are used to calculate the deflections and rotations in two principal directions of the sections along the length of the column.

$$\delta_{xl} = \sum_{p=1}^{p=l} \left[\theta_{xp} + \left(\phi_{xp} + 2\phi_{x(p-1)} \right) dh/6 \right] dh, \quad (76)$$

$$\delta_{yl} = \sum_{p=1}^{p=l} \left[\theta_{yp} + \left(\phi_{yp} + 2\phi_{y(p-1)} \right) dh/6 \right] dh, \quad (77)$$

$$\theta_{xl} = \sum_{p=1}^{p=l} \left[\left(\phi_{xp} + 2\phi_{x(p-1)} \right) / 2 \right] dh, \quad (78)$$

$$\theta_{yl} = \sum_{p=1}^{p=l} \left[\left(\phi_{yp} + 2\phi_{y(p-1)} \right) / 2 \right] dh, \quad (79)$$

where $dh = L/p$; L represents the length of column; p represents the number of sections considered along the column; ϕ_{xp} and ϕ_{yp} represent the curvatures in two principal directions of section number p ; δ_{xl} and δ_{yl} represent the deflections of section l in the x and y directions, respectively; θ_{xl} and θ_{yl} represent rotations of section l in the x and y directions, respectively.

The deflections in two principal directions (δ_{xl} and δ_{yl}) are calculated and then, the deflection resultant is calculated.

The second option (EPM) is based on the evidence that a column is highly affected in the critical zone when a lateral load is applied. Immediately following the peak value of the $M-\phi$ curve of the critical section, a very important local effect occurs at the critical section where a pseudo-plastic hinge appears. Once the peak has passed, curvature enhancement is concentrated in the critical zone. While in the other regions, the curvatures decrease rapidly to near zero.

In this paper, the column's deflections are calculated using EPM [15]. When applying EPM to calculate deflections, Eqs. (80) and (81) are used:

$$\delta = \left(\frac{\phi}{3} L^2 \right) \quad (\text{for } \phi \leq \phi_p), \quad (80)$$

$$\delta = \left(\frac{\phi_p}{3} L^2 \right) + (\phi - \phi_p)(L_p)(L - 0.5L_p) \quad (\text{for } \phi \geq \phi_p), \quad (81)$$

where δ represents the deflection at the top of ME (half-column); ϕ represents the curvature at the critical section and ϕ_p represents its value at the plastic hinge performance phase, respectively; L and L_p represent the lengths of ME and the length of plastic hinge, respectively.

There is a good agreement between simulated deflections by applying both mentioned methods and the

experimental results in the elastic phase. In the post-elastic phase, CNDIM underestimates the deflection values, while there is good agreement between the experimental results and simulated deflections using EPM.

3.2 Computer Programming

A computer program entitled Cyclic Biaxial Bending Column Simulation (CBBCS) has been developed by the author to simulate numerically the behavior of RC columns under CBBMAL, considering the nonlinear behavior of materials. CBBCS takes into account the confining effect of the transverse reinforcements and simulates the loss of the concrete cover. It allows the determination of the failure, the internal local behavior of critical sections (strains, stresses, neutral axis position, cracks positions, loss of material, microscopic damage index, etc.) and the external global behavior of the column (curvature, deflection, stiffness, damping ratio, macroscopic damage index [16], etc.).

Figure 4 shows a flowchart of the main parts of the proposed simulation method.

4 Experimental Data and Reference Column

The proposed numerical simulation has mainly been validated by the experimental test results of Garcia Gonzalez performed on the full-scale columns [17–19] and the experimental tests/simulation of Park [11].

The dimensions and characteristics of the columns tested by Garcia Gonzalez are as follows: rectangular sections 18 cm \times 25 cm, height of 1.75 m, four longitudinal reinforcement with a diameter of 12 mm, concrete of strength of 42 MPa, stirrup ties of diameter 6 mm with a longitudinal spacing of 9 cm, yielding stress of steel bars 470 MPa. This column is fixed at the bottom, free at the top and is under an axial force of 500 kN and cyclic or monotonic lateral force at the top. The horizontal loads through different orientation angles Ω have been applied on the top of the columns. In this paper, Garcia Gonzalez's column is called "reference column" and its section is called "reference section".

5 Assessment of the Obtained Results

Comparison of numerically simulated results using the proposed simulation algorithm and experimental tests on full-scale RC members is reflected in Figs. 5, 6, 7, 8 and 9. The comparison indicates a good agreement between the proposed simulation and the experimental test results.

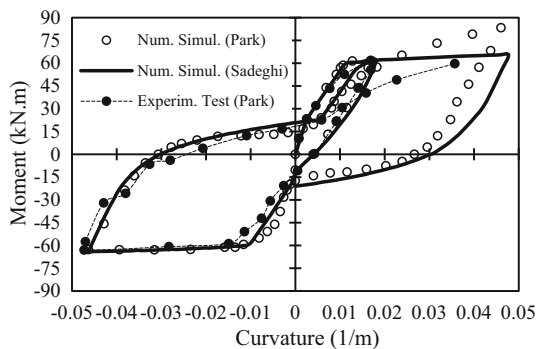


Fig. 5 Comparison of the proposed simulation and experimental test/simulation of Park, CBM case

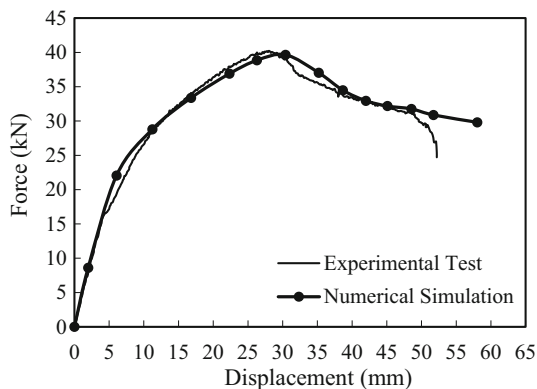


Fig. 6 Comparison of the proposed simulation and experimental tests results, BMAL case ($\Omega = 0^\circ$)

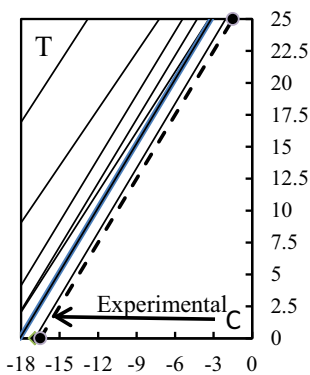


Fig. 7 The neutral axis positions of the reference section under BBMAL, $\Omega = 45^\circ$

In Fig. 5, the results of the proposed simulation and experimental test/simulation of Park for a cyclic bending moment (CBM) loading case are compared. As this figure shows, there is a good agreement between the simulated and experimental results.

In Fig. 6, the results of the proposed simulation are compared with the experimental test results [17] on the

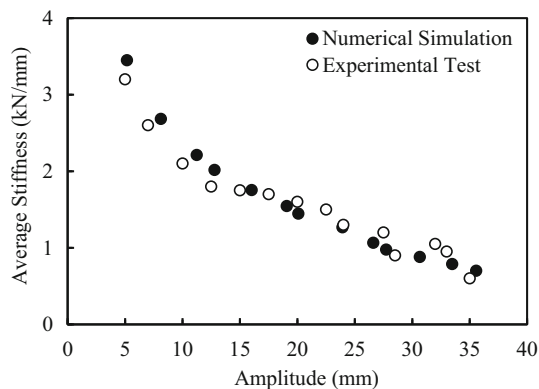


Fig. 8 Comparison of the simulated and tested average stiffness's, CBBMAL, $\Omega = 30^\circ$

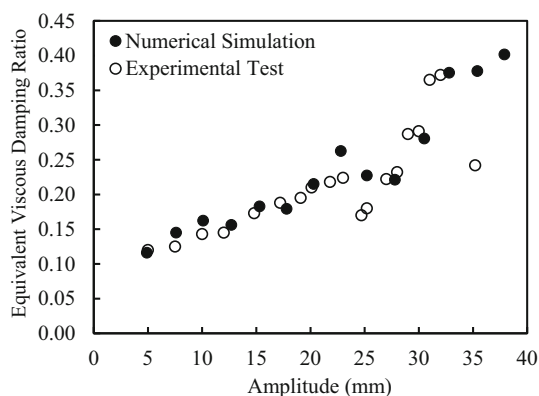


Fig. 9 Comparison of the simulated and tested equivalent viscous damping ratios, CBBMAL, $\Omega = 30^\circ$

reference column under bending moment and axial loading (BMAL) with the orientation angle of $\Omega = 0^\circ$.

Figure 7 shows the variations of the position of the neutral axis at the critical section of the reference column when BBM loading with the orientation angle of $\Omega = 45^\circ$ is increased to its maximum value. Note that only for illustration purposes, the values on x axis are shown in the negative form in Fig. 7. As shown in this figure, by increasing BBM, the neutral axis moves from outside the section to point T with an inclination of about $\alpha = 55^\circ$ and then shifts toward the center of the section with an inclination of $\alpha = 60^\circ$ when the maximum load is applied.

When the load is increased, the neutral axis moves with an approximately constant inclination up to the ultimate strength of the section. The results of measurements on the full-scale experimental tests [17] for the neutral axis position, when peak load is applied on the critical section of the reference column, are shown by the dashed lines in Fig. 7. Experimental test results showed an inclination of $\alpha = 59^\circ$ for the neutral axis when peak load was applied on the section for an orientation angle of $\Omega = 45^\circ$. As Fig. 7

shows, there is a good agreement between the simulated values and experimental results.

Figures 8 and 9 compare the simulated values and experimental test results [17] of average stiffness and equivalent viscous damping ratio for CBBMAL.

Figure 10 shows the variations of the $M-\phi$ curves of the critical section of the reference column under BBMAL for different values of axial force “Next” for the pushover orientation angle of $\Omega = 30^\circ$. As this figure indicates, the stiffness and ultimate strength of the column are increased by increasing the axial force. Also, it shows that the failure of the column occurs earlier by increasing the axial force, meaning a heavy axial load makes the column fragile, imposing a big loss of material and reducing the ductility of the column. This type of fragility, reduction of ductility and loss of material need to be carefully considered in prestress structural member design. Similarly, care needs to be taken in the design of structures being designed for seismic zones having a significant vertical force component of earthquake loading.

Figure 11 presents the axial force–moment interaction diagram of the reference section under different orientation angles Ω . Figure 12 presents the axial force–moment interaction diagram for the critical section of the reference column under BMAL with the orientation angle of $\Omega = 0^\circ$ for different slenderness ratios (h/L) of the column. As these figures indicate, the function of axial force in combination with flexural moment in the damage of the section located beyond or below the balance point in the interaction diagram is principally different. For the latter condition, axial load progresses damage more due to reduction of capacity terms. However, sometimes the influence of axial load compensates reduction of capacity and consequently the damage decreases. In compression control region of interaction diagram, as far as yield strength is not attained, damage is not obtained, whereas beyond this margin, increase in axial load definitely leads to sudden failure of element, as confirmed by Abbasnia et al. [20].

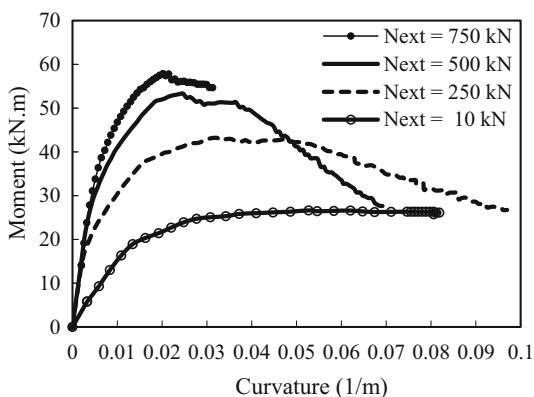


Fig. 10 Effect of axial force on the response of the critical section under BBMAL, $\Omega = 30^\circ$

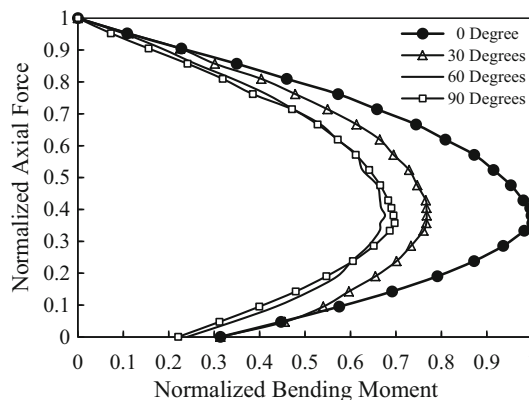


Fig. 11 Interaction diagram of reference section under different orientation angles Ω

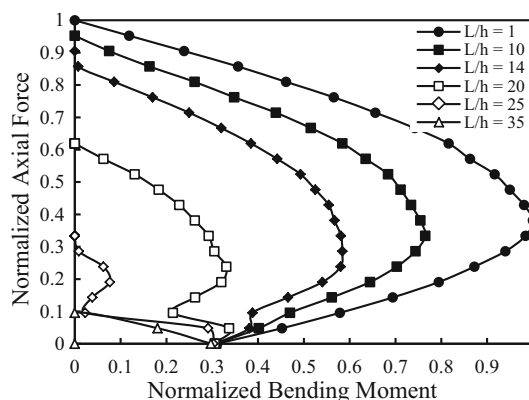


Fig. 12 Interaction diagram for different slenderness ratios of full-size columns, $\Omega = 0^\circ$

6 Verification of the Components Effects Combination Method (CECM)

In seismic zones, the building codes generally accept the use of the combination of the components’ effects in linear and equivalent linear calculations. As an example, according to French earthquake code (AFPS) [21], in nonlinear calculations, the three components are to be considered simultaneously in calculation, but in linear and equivalent linear calculations, the maximum effect of each component can be determined separately and then combined according to the following formulation:

$$S = \mp S_x \mp \lambda S_y \mp \mu S_z, \tag{82}$$

$$S = \mp \lambda S_x \mp S_y \mp \mu S_z, \tag{83}$$

$$S = \mp \lambda S_x \mp \mu S_y \mp S_z, \tag{84}$$

where S_x , S_y and S_z represent the deformations or loading due to the horizontal and vertical components, respectively, and S represents their resultant values.

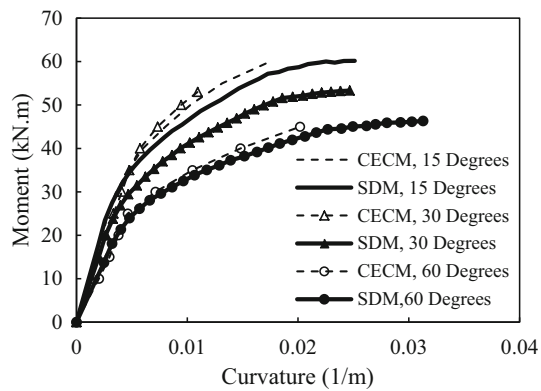


Fig. 13 Comparison of CECM and SDM for orientation angles Ω of 15°, 30° and 60°

In general cases, λ and μ are taken equal to 0.4. The effect of the vertical component can be neglected ($\mu = 0$ and the third equation, i.e., Equation (84) is neglected).

The application of this simplified method (CECM) is compared with the proposed simultaneous direct method (SDM). To carry out this comparison, the responses of the critical section of the reference column under BBMAL for different orientation angles have been studied.

Figure 13 shows the $M-\phi$ curves of the critical section of the reference column under BBMAL with orientation angles of $\Omega = 15^\circ, 30^\circ$ and 60° for both cases of calculation methods: CECM (according to AFPS) and SDM. Note that only the calculations up to the ultimate strength of the section are shown in Fig. 13.

In the linear phase, there is a very good agreement between the results obtained from SDM and CECM for all orientation angles (Ω) (i.e., different ratios of M_y and M_x), as confirmed by AFPS.

In the post-elastic phase, CECM presents an underestimation of the response, which is not conservative. The maximum underestimation of the response is observed when the resultant moment is applied in the diagonal direction of the section.

The obtained results show the necessity of applying SDM for nonlinear calculations, especially during the post-elastic phase, which occurs frequently during earthquake loading.

7 Conclusions

A nonlinear numerical simulation algorithm has been proposed to simulate the behavior of RC columns subjected to CBBMAL. In the proposed simulation algorithm, the column is decomposed into two ME positioned between the inflection point and critical sections. Then the nonlinear behavior of ME is analyzed and, finally, the two connected

ME are assembled to determine the global behavior of the column. To find the status of the entire column, the applied loads and also the secondary moments, due to P- Δ effect, are considered in the simulation of the column.

A computer program has been developed to simulate numerically the behavior of RC columns under CBBMAL, considering the nonlinear behavior of the materials. It takes into account the confining effect of the transverse reinforcements and simulates the loss of the concrete cover, and allows the determination of the failure, the internal local behavior of critical sections and the external global behavior of the column.

The proposed nonlinear numerical solution has been validated by experimental test results. A comparison of the numerically simulated results using the proposed simulation algorithm and the experimental tests on full-scale RC members indicates a good agreement between the proposed simulation and the experimental test results.

The comparison between SDM and CECM shows that in the elastic phase, for all the values of applied resultant moment in BBMAL cases, there is a very good agreement between SDM and CECM, as confirmed by AFPS. In the post-elastic phase, CECM presents an underestimated response, which is not conservative and as such should be used with due caution. The maximum underestimation of the response is observed when the resultant moment is applied in the diagonal direction of the section. The obtained results show the necessity of applying SDM for nonlinear calculations, especially during the post-elastic phase, which occurs frequently during earthquake loading.

Acknowledgments The financial and technical supports of the Near East University and University of Nantes/Ecole Central de Nantes are appreciated.

References

- Richard Yen JY (1991) Quasi-Newton method for reinforced concrete column analysis and design. *J Struct Struct Div ASCE* 117(3):657–666
- Yau CY, Chan SL, So AKW (1993) Biaxial bending of arbitrarily shaped reinforced concrete column. *Struct J ACI Tech Paper* 90(3):269–273 **Title no. 90-S28**
- Alnoury SI, Chen WF (1982) Behavior and design of reinforced and composite concrete sections. *J Struct Div ASCE* 108(ST6):1266–1284
- Hsu CT, Mirza S (1973) Structural concrete biaxial bending and compression. *J Struct Div ASCE* 99(ST2):2317–2335
- Brondum-Nielsen T (1985) Ultimate flexural capacity of cracked polygonal concrete sections under biaxial bending. *J ACI* 82–80:863–869 **Technical Paper, no. 82–80**
- Zak L (1993) Computer analysis of reinforced concrete sections under biaxial bending and longitudinal load. *S J ACI* 90(2):163–169

7. Amziane S, Dubé JF (2008) Global RC structural damage index based on the assessment of local material damage. *J Adv Concr Technol* 6(3):459–468
8. Sadeghi K (1995) Simulation numérique du comportement de poteaux en béton armé sous cisaillement dévié alterne, Ph.D. dissertation, University of Nantes/Ecole Central de Nantes
9. Sadeghi K (2002) Numerical simulation and experimental test of compression confined and unconfined concrete. Technical report submitted to Water Resources Management Organization, Ministry of Energy, Concrete Laboratory of Power and Water University of Technology, Tehran
10. Sadeghi K (2014) Analytical stress-strain model and damage index for confined and unconfined concretes to simulate rc structures under cyclic loading. *Int J Civil Eng* 12(3):333–343
11. Park R, Kent DC, Sampson RA (1972) Reinforced concrete members with cyclic loading. *J Struct Div Proc Am Soc Civil Eng* ST7:1341–1359
12. Comité Euro-International du béton, Code-Modèle CEB-FIP pour les structures en béton, Bulletin d'information no. 124–125F, vol. 1 and 2, April, Paris (1978)
13. Sheikh SA (1982) A comparative study of confinement models. *ACI J* 79(4):296–305
14. Lamirault J (1984) Contribution à l'étude du comportement des ossatures en béton armé sous cisaillement normales. Simulation par analyse non linéaire globale, Ph.D. Dissertation, University of Nantes/Ecole Central de Nantes, Nantes
15. Priestley MJN, Park R (1991) Strength and durability of concrete bridge columns under seismic loading. *Struct J ACI* 88(4):61–76
16. Sadeghi K (2011) Energy based structural damage index based on nonlinear numerical simulation of structures subjected to oriented lateral cyclic loading. *Int J Civil Eng* 9(3):155–164
17. Garcia Gonzalez JJ (1990) Contribution à l'étude des poteaux en béton armé soumis à un cisaillement dévié alterné, Ph.D. dissertation, University of Nantes/Ecole Central de Nantes
18. Sieffert JG, Lamirault J, Garcia Gonzalez JJ (1990) Behavior of R/C columns under static compression and lateral cyclic displacement applied out of symmetrical planes. *Structural Dynamics*, vol 1, Kratzig et al., Balkema, Rotterdam, pp 282–293
19. Sadeghi K, Lamirault J, Sieffert JG (1993) Damage indicator improvement applied on R/C structures subjected to cyclic loading. In: Proceedings of the 2nd European conference on structural dynamics (EURODYN 93), Trondheim, *Structural Dynamics*, vol. 1, pp 129–136
20. Abbasnia Reza, Mirzadeh Neda, Kildashti Kamyar (2011) Assessment of axial force effect on improved damage index of confined RC beam-column members. *Int J Civil Eng* 9(3):237–246
21. AFPS90, Combinaison des effets des composantes du mouvement sismique, Recommandations AFPS90 pour la rédaction de règles relative aux ouvrages et installations à réaliser dans les régions sujettes aux séismes, AFPS, 101-105, Paris (1990)